Synthesis and Biological Evaluation of Dimeric RGD Peptide−Paclitaxel Conjugate as a Model for Integrin-Targeted Drug Delivery

Xiaoyuan Chen,[†,§,*] Carmen Plasencia,[‡] Yingping Hou,[†] and Nouri Neamati[‡,*]

Department of Radiology and Department of Pharmaceutical Sciences, University of Southern California, Los Angeles, California 90033, and Molecular Imaging Program at Stanford, Department of Radiology, Stanford University, Stanford, California 94305

Received October 18, 2004

Targeting drugs to receptors involved in tumor angiogenesis is a novel and promising approach to improve cancer treatment. In this study, we evaluated the antitumor activity of paclitaxel (PTX) conjugated with a bicyclic peptide E[c(RGDyK)]$_2$ (RGD) in a metastatic breast cancer cell line (MDA-MB-435). The cyclic RGD peptide selectively binds to α_v integrin receptors that are highly expressed in metastatic cancer cells. PTX, an antimicrotubule agent, is a potent antitumor agent commonly used in the treatment of advanced metastatic breast cancer. The in vitro results showed that RGD peptide inhibited cell cycle proliferation by arresting cells in G_0/G_1-phase. The PTX−RGD conjugate inhibited cell proliferation with activity comparable to that observed for paclitaxel, both of which were mediated by an arrest of G_2/M-phase of the cell cycle followed by apoptosis. Although the PTX−RGD conjugate showed slightly decreased integrin binding affinity than the unconjugated peptide, it indicated integrin specific accumulation in vivo. ^{125}I-Labeled PTX−RGD showed highest tumor uptake at 2 h postinjection (2.72 ± 0.16%ID/g) and best tumor/background contrast after 4 h postinjection. Our results demonstrate the potential of tumor-targeted delivery of paclitaxel based on the specific recognition of cell adhesion molecule $\alpha_v\beta_3$ integrin to reduce toxicity and enhance selective killing of cancer cells.

Introduction

The efficacy of chemotherapeutic drugs is limited by low sensitivity for tumor cells and high toxicity to healthy tissues.[1,2] The activity of most chemotherapeutic agents is further limited by the development of drug resistance. Tumor cells are a rapidly changing target because of their genetic instability, heterogeneity, and high rate of mutation, leading to selection and overgrowth of a drug-resistant tumor cell population.[3] To increase the therapeutic index, various drug delivery systems are being developed. Most carriers mainly focus on macromolecules such as monoclonal antibodies, proteins, or peptides. Hybrid molecules designed to bind to specific, overexpressed receptors on tumor cells are an attractive avenue for selective targeting.[4,5]

Angiogenesis, the formation of new blood vessels from preexisting vasculature, is essential for tumor growth and progression.[6,7] Inhibition of angiogenesis has been shown to prevent tumor growth and even causes tumor regression in various experimental models.[8] In contrast to traditional chemotherapeutics, which target all dividing cells, antiangiogenic therapy selectively targets activated endothelial and tumor cells. In early Phase I/II clinical trials, angiogenic modulators have shown modest toxicity, were cytostatic, slowed tumor growth and metastasis, and produced an objective remission.[9] However, antiangiogenic therapy with the aim to normalize tumor vasculature usually is not sufficient to eradicate tumors in the late stage.[8−10] Thus, combinations of antiangiogenic agents with either chemo- or radiation therapy has demonstrated enhanced antitumor activity in multiple tumor systems, and its effectiveness has been shown in breast cancer models.[11−13] The synergy most likely results from the impact of antiangiogenesis that decreases the interstitial tumor pressure leading to improved blood flow with subsequent improved local delivery when given systemically.[13]

The expression of integrin adhesion molecules $\alpha_v\beta_3$ and $\alpha_v\beta_5$ on sprouting capillary cells and their interaction with specific matrix ligands play a key role in angiogenesis and metastasis.[14] The α_v integrin receptors are highly expressed on activated endothelial cells and tumor cells, but not expressed in resting endothelial cells and most normal organ systems, making it a potential target for antiangiogenic strategy. Inhibition of α_v integrin activity by mAbs, cyclic RGD peptides, and peptidomimetics has been shown to induce endothelial apoptosis,[15] inhibit angiogenesis,[16,17] and increase endothelial monolayer permeability.[18] Suitably radiolabeled RGD peptides have also been developed for noninvasive imaging of integrin expression during tumor angiogenesis, growth, and spread.[19−29]

X-ray crystallographic structures of the extracellular segment of $\alpha_v\beta_3$ integrin and its complex with cyclic RGD peptide c(RGDf[NMe]V) revealed electrostatic interactions between the peptide ligand and the $\alpha_v\beta_3$

* Corresponding authors. Xiaoyuan Chen, Ph.D.; Molecular Imaging Program at Stanford, Department of Radiology, Stanford University School of Medicine, 300 Pasteur Dr., Edwards Bldg. R354, Stanford, CA 94305-5344. Phone: (650)725−0950; Fax: (650)736−0234; E-mail: shawchen@stanford.edu. Nouri Neamati, Ph.D.; Department of Pharmaceutical Sciences, School of Pharmacy, University of Southern California, 1985 Zonal Ave., Rm. 304, Los Angeles, CA 90089. Phone: 323-442-2341; Fax: 323-442-1390; E-mail: neamati@usc.edu.

† Department of Radiology, University of Southern California, Los Angeles.

‡ Department of Pharmaceutical Sciences, University of Southern California, Los Angeles.

§ Department of Radiology, Stanford University.

10.1021/jm049165z CCC: $30.25
Published on Web 01/27/2005

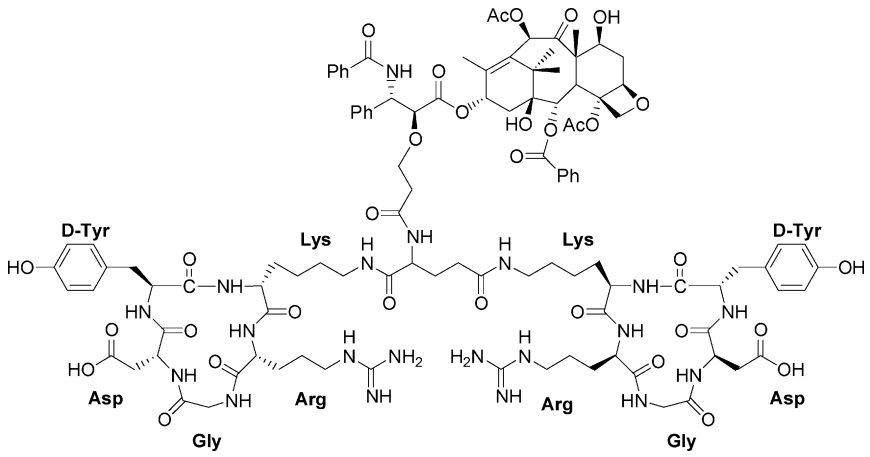

Figure 1. Schematic representation of the molecular structure of dimeric RGD peptide−paclitaxel conjugate. The succinate linkage is through the 2′-hydroxy group of paclitaxel and amino group of RGD glutamate residue.

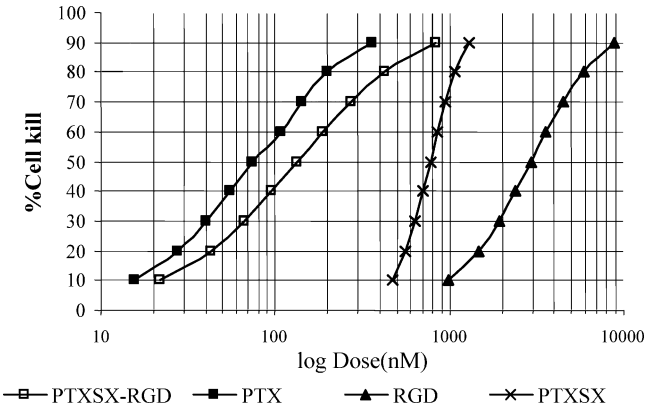

Figure 2. Cytotoxic effect of PTX, PTXSX, PTX−RGD conjugate, and RGD peptide. MDA-MB-435 cells were treated with continuous exposure of each drug for 48 h, and cytotoxicity was assessed by MTT assay as described in the Experimental Section. Data are presented as a measure of percent survival normalized against the untreated population. Each data point is from an average of three to four independent experiments performed in triplicate. IC_{50} values for PTX, PTXSX, PTX−RGD, and RGD are 34 ± 5, 67 ± 9, 134 ± 28, and 2940 ± 15 nM, respectively.

receptor: arginine interacts with two anionic aspartic acid residues in the α-subunit, aspartic acid interacts with divalent metal cation in the metal ion-dependent adhesion site (MIDAS) region of the β-subunit, and glycine forms close contact with the protein. D-Phenylalanine is involved in hydrophobic interactions, while *N*-methylvaline forms no contact with the protein.[30−32] Thus, we have changed D-Phe to D-Tyr to increase hydrophilicity, as well as providing the possibility of iodination radiolabeling. *N*-Methylvaline was changed to lysine to facilitate further modification via the side chain ϵ-amino group.[19−23,26] It was also recently reported that dimeric and multimeric cyclic RGD peptides have higher receptor binding affinity in vitro[33] and better tumor retention in vivo.[24,25,29] This is presumably due to polyvalency, which gives rise to an enhanced binding and steric stabilization.[34]

Estrogen-independent breast cancer cell line MDA-MB-435 is known to express high levels of integrin $\alpha_v\beta_3$, and the expression of activated $\alpha_v\beta_3$ integrin has been associated directly with the metastatic and osteolytic potential of MDA-MB-435 breast carcinoma.[25,35,36] In this study, we used dimeric RGD peptide $E[c(RGDyK)]_2$, a potent α_v-integrin antagonist, as carrier for paciltaxel to specifically target breast cancer cells and tumor blood vessels. The in vitro receptor binding, cytotoxicity, and apoptosis results were observed in the MDA-MB-435 cell line, and biodistribution data was performed in an orthotopic nude mouse breast cancer model.

Results

Synthesis and Characterization. The conjugate of paclitaxel (PTX) with dimeric RGD peptide[37] (Figure 1) was prepared by derivatizing the 2′-hydroxy function of paclitaxel with succinic anhydride, according to reported procedure.[38] The paclitaxel hemisuccinate ester (PTXSX) was activated using EDC and NHS, followed

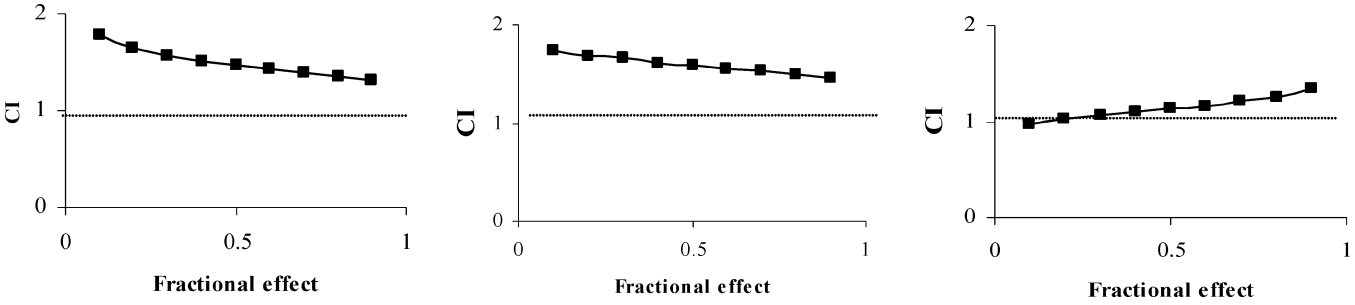

Figure 3. Combination index (CI) for PTX and RGD combinations. MDA-MB-435 cells were treated with various IC_{50}:IC_{50} ratios of PTX and RGD. (Left panel) PTX+RGD: simultaneous exposure of both drugs for 48 h. (Middle panel) PTX→RGD: cells were pretreated with PTX for 24 h, and then RGD was added for an additional 24 h. (Right panel) RGD→PTX: cells were exposed to RGD for 24 h, and then PTX was added for an additional 24 h. The fractional effect was evaluated by Chou−Talalay method. CI = 1 reflects additive effects, CI > 1 antagonism and CI < 1 synergism.

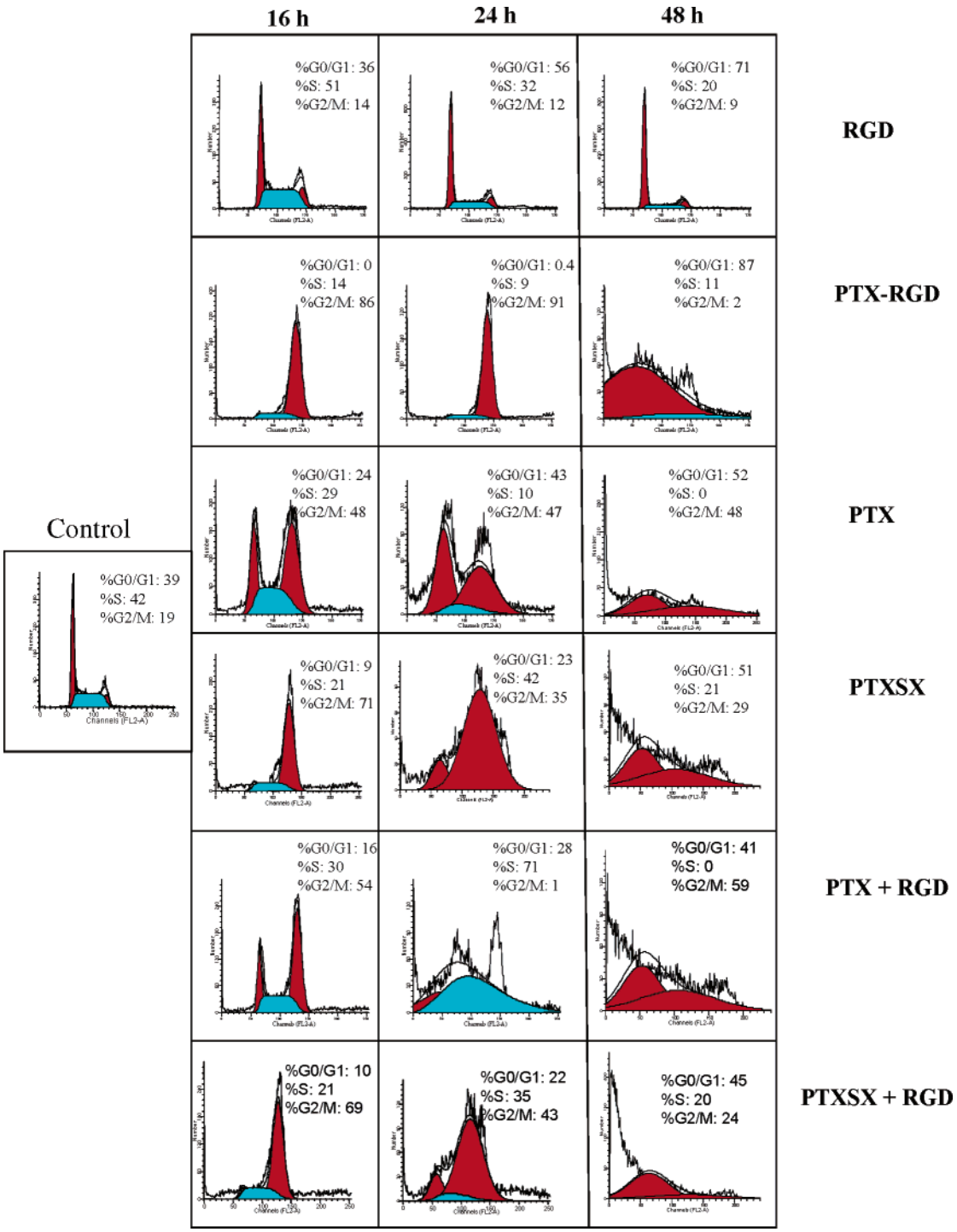

Figure 4. Flow cytometric analysis of the cell cycle profiles of treated MDA-MB-435 cells. RGD peptide induces cell cycle arrest in G_0/G_1 phase with no apoptosis even at high drug concentration and prolonged exposure. All three PTX derivatives resulted in G_2/M cell cycle arrest with distinct apoptosis (sub-G_0/G_1 population) 24 h after drug treatment.

by coupling with RGD peptide glutamate amino group under slightly basic conditions.

Cytotoxicity Assessments. The cytotoxic effect of PTX, PTXSX, RGD, and PTX−RGD conjugate administered as single agents was assessed by MTT (3-(4, 5-dimethylthiazole-2-yl)-2,5-diphenyltetrazoliumbromide) assay[39] in MDA-MB-435 breast cancer cells after 48 h continuous drug exposure (Figure 2). PTXSX with the IC_{50} of 67 ± 9 nM showed similar potency to PTX (IC_{50} = 34 ± 5 nM). However, PTX−RGD conjugate with the IC_{50} value of 134 ± 28 nM was slightly less potent than free PTX. Cyclic RGD peptide was the least potent (IC_{50} = 2.9 ± 0.1 μM).

Analysis of Drug Combinations. Sequential and concomitant combinations of PTX and RGD peptide were analyzed in MDA-MB-435 cells by the method of Chou and Talalay.[40] We observed that simultaneous (schedule 1) and sequential PTX treatment followed by RGD (PTX → RGD, schedule 2) produced antagonistic effects (CI > 1; Figure 3). However, when cells were exposed to RGD before the addition of PTX (RGD → PTX, schedule 3), an additive effect was observed at all

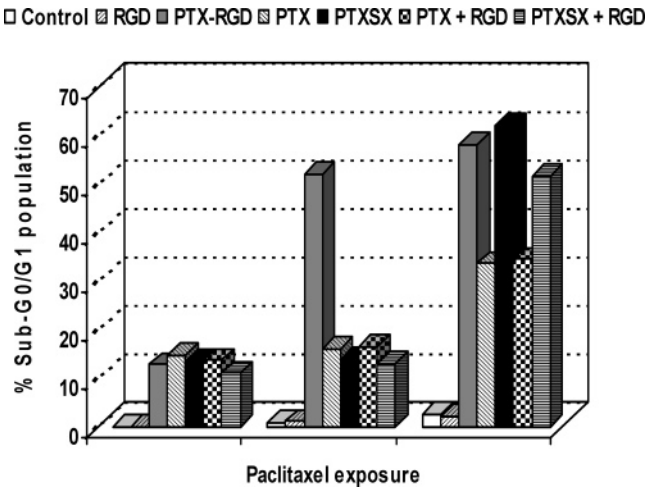

Figure 5. Percentage of sub-G_0/G_1 population determined by flow cytometry. The PTX−RGD conjugate is comparable to that of PTX/RGD combination.

levels of fractional inhibition. As shown in Figure 3, previous exposure to RGD reduced the PTX dose given in combination as compared to PTX administered as a single agent. The cytotoxicity of the simultaneous combination between PTXSX and RGD was also evaluated. In contrast to the data obtained for PTX, a modest synergistic effect was observed for PTXSX and RGD combination (data not shown).

Effect on Cell Cycle Progression. Flow cytometric analysis was performed to analyze the cell cycle perturbations and apoptosis. As expected, RGD administered as a single agent induced cell cycle arrest in G_0/G_1 phase. No apoptotic fraction (as determined by the sub-G_1 peak) was observed even at longer exposures to high concentrations of the drug (IC_{80}, Figure 4), which correlates well with the cytostatic effect observed in the drug sensitivity test. A G_2/M cell cycle arrest was observed for PTX, PTXSX, and PTX−RGD conjugate (Figure 4). The appearance of apoptotic cells (as calculated by sub-G_0/G_1 population) was evident at 24 h for all drugs. PTX−RGD conjugate and PTXSX showed similar mitotic arrest and apoptotic cell death to that of PTX. In all cases, the apoptotic events seemed to occur after G_2/M arrest (Figure 5).

Simultaneous combination of PTX, PTXSX, and RGD first induced a slight G_2/M-phase arrest at 16 h followed by the progressive appearance of a sub-G_1 peak characteristic of apoptosis (Figure 5). Levels of apoptotic fractions increased up to 35% and 57% with PTX/RGD and PTXSX /RGD combination, respectively (Figure 5). Our findings also demonstrate that the PTX−RGD conjugate is as efficacious as the combination of PTX or PTXSX and RGD.

Characterization of Drug-Induced Apoptosis. An early event in apoptotic cell death is the translocation of the phosphatidyl-serine (PS) residues to the outer part of the cytoplasmatic cell membrane. In the presence of calcium, rapid high affinity binding of annexin V to PS occurs. PS translocation to the cell surface precedes nuclear breakdown, DNA fragmentation, and the appearance of most apoptosis-associated molecules, making annexin V binding a marker of early-stage apoptosis. By using this method, we determined the ability of PTX−RGD conjugate to induce apoptosis and compared it to the ability of PTX and RGD used as a single agents or in simultaneous combination (PTX+RGD). As shown in Figure 6, PTX−RGD conjugate caused a strong apoptotic effect comparable to that induced by PTX as a single agent. At 24 h, 12% of PTX−RGD conjugate-treated cells appeared to be in early apoptosis as compared to 17% for PTX. An increase in late apoptosis/necrosis was also apparent at 48 h for both drugs (Figure 6). No significant changes in the percentage of apoptotic cells were observed in RGD treated cells, data that correlates with the results obtained in the cell cycle analysis. Moreover, as we previously observed in the cell cycle profile for the simultaneous combination of PTX and RGD, the presence of RGD significantly reduced the percentage of apoptotic cells as compared to PTX−RGD as a single agent.

Integrin Binding Affinity. To determine whether PTX conjugation alters the receptor affinity of dimeric RGD peptide, competitive binding measurements were performed between ^{125}I-echistatin and the RGD peptide ligands (Figure 7). All ligands tested in these assays showed the expected sigmoid curves. Coupling of a rather bulky PTX moiety with dimeric RGD peptide through the succinate tether did not significantly reduce the receptor avidity of the peptide (IC_{50} values for $E[c(RGDyK)]_2$ and PTX−RGD conjugate were 15.6 and 25.9 nM, respectively).

Biodistribution. To assess the effect of conjugation and the presence of drug moiety on the MDA-MB-435 tumor and normal tissue uptake, the biodistribution of the ^{125}I-labeled conjugate (^{125}I-RGD−PTX) was compared to that of ^{125}I-RGD. Radioiodination of both compounds through a standard Chloramine-T method afforded the labeled molecules as evidenced by radio-HPLC with high specific activity (1500 to 2000 Ci/mmol). Typical radiochemical yield after HPLC purification for both radioligands was about 50−60% with radiochemical purity over 95%. The labeled RGD and conjugate were injected intravenously (iv) into athymic nude mice carrying orthotopic MDA-MB-435 xenografts. Tissues were removed at different time-points postinjection (pi) and the radioactivity uptakes, expressed in %ID/g were measured (Tables 1 and 2). Both RGD and PTX−RGD conjugate revealed fast blood clearance. Tumor activity accumulation was rapid for ^{125}I-RGD (e.g., 3.85 ± 1.15% ID/g at 30 min pi) and was quickly washed out, resulting in only 1.64 ± 0.24%ID/g at 4 h pi. The maximum tumor uptake for the conjugate appeared at 2 h pi (2.72 ± 0.16%ID/g), and remained constant at 4 h pi (2.37 ± 0.76%ID/g). The best tumor-to-blood and tumor-to-muscle ratios were achieved after 4 h pi. To demonstrate that the RGD and RGD−PTX conjugate uptakes in MDA-MB-435 tumors were specific and receptor mediated, biodistribution studies were performed by co-injecting of c(RGDyK) (10 mg/kg) with the iodinated radiotracers. Uptake values of 0.87 ± 0.17 and 0.42 ± 0.07%ID/g were observed at 1 h pi for RGD and the conjugate, respectively. These values were 4−5 times lower than the tumor uptake of the radiotracers when no blocking agent was co-injected.

Discussion

In the present work, a dimeric RGD peptide $E[c(RGDyK)]_2$ was conjugated to paclitaxel (PTX) and evaluated

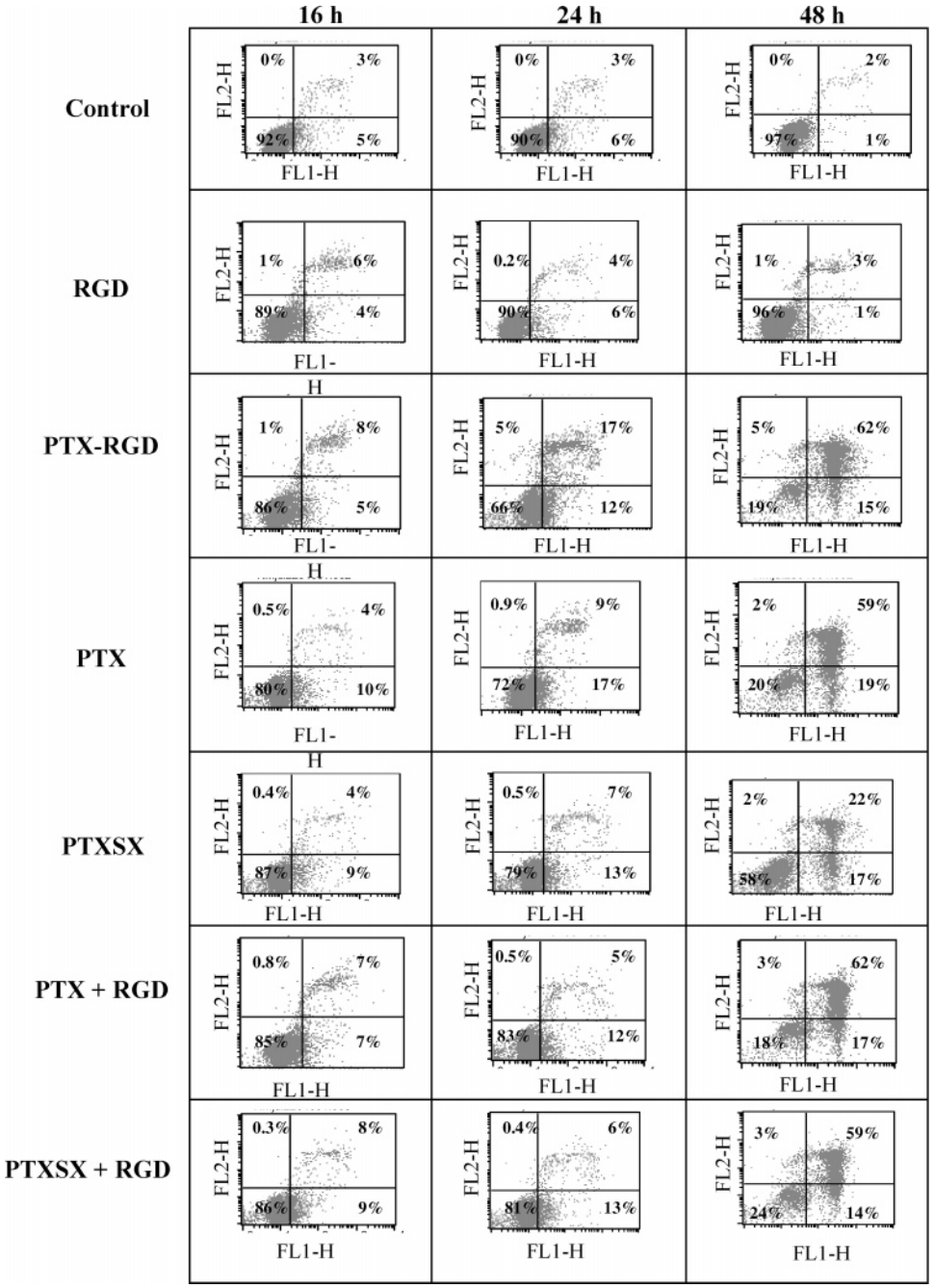

Figure 6. Apoptosis analysis of MDA-MB-435 cells treated with RGD, PTX−RGD, PTX, PTXSX, and simultaneous combination of PTX and PTXSX with RGD. Cells stained with annexinV/propidium iodide and analyzed by flow cytometry.

for its in vitro antiproliferative effect in comparison with free PTX and for its in vivo tumor-targeting efficacy. We showed that PTX−RGD conjugate inhibits tumor cell growth comparable to that of PTX and PTXSX. PTX−RGD inhibition of cell growth was mediated by cell cycle retention and apoptosis. PTX−RGD blocked cell cycle in G_2/M-phase, with the subsequent disappearance of the G_0/G_1 and S peaks, which was comparably similar to that induced by PTX and PTXSX. The cell cycle arrest induced by these compounds (PTX, PTXSX, and PTX−RGD) was followed by cell death, as determined by annexin V/PI staining. Moreover, PTX−RGD conjugate caused a very strong apoptotic effect. At 24 h, 17% of PTX−RGD conjugate treated cells appeared to be in early apoptosis compared to 9% for PTX. These data is consistent with the increase in the

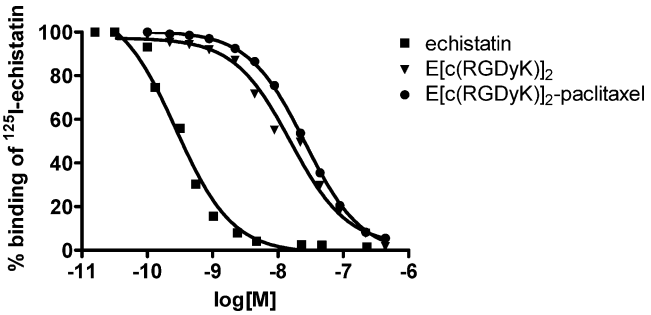

Figure 7. Competition of specific binding of ^{125}I-echistatin with unlabeled echistatin (■), E[c(RGDyK)]$_2$ (▼), and PTX−E[c(RGDyK)]$_2$ conjugate (●) to MDA-MB-435 cells. Cell-associated radioactivity in the absence of competitor was set at 100%. Values are mean of triplicate assays ± SD. [echistatin: 0.28 nM; RGD: 15.6 nM; RGD−PTX: 25.9 nM].

Table 1. Radioactivity, Expressed as Percent Injected Dose per Gram Tissue in Different Organs and Tumor of MDA-MB-435 Xenograft Model after Intravenous Injection of 2 μCi of ^{125}I-E[c(RGDyK)]$_2$ at 30 min, 1, 2, 4 h, and 1 h Block (with coinjection of 10 mg/kg c(RGDyK)) (n = 4)

	0.5 h	1 h	2 h	4 h	1 h block
blood	1.82 ± 0.43	0.95 ± 0.04	0.52 ± 0.09	0.16 ± 0.04	1.16 ± 0.31
muscle	0.77 ± 0.23	0.57 ± 0.01	0.44 ± 0.02	0.32 ± 0.07	0.62 ± 0.44
tumor	3.85 ± 1.15	2.91 ± 0.35	2.44 ± 0.10	1.64 ± 0.24	0.87 ± 0.17
bone	1.49 ± 0.63	1.05 ± 0.15	0.81 ± 0.19	0.49 ± 0.14	0.56 ± 0.01
heart	1.28 ± 0.31	0.83 ± 0.01	0.68 ± 0.01	0.36 ± 0.03	0.62 ± 0.14
lung	3.30 ± 0.94	1.99 ± 0.08	1.43 ± 0.15	0.97 ± 0.08	1.47 ± 0.24
liver	2.64 ± 0.77	2.30 ± 0.17	2.11 ± 0.08	1.13 ± 0.05	1.29 ± 0.24
kidney	10.1 ± 1.10	8.95 ± 0.82	8.01 ± 0.64	5.65 ± 0.09	6.43 ± 0.91
spleen	1.96 ± 0.57	1.60 ± 0.07	1.44 ± 0.09	0.85 ± 0.01	0.89 ± 0.37
pancreas	0.57 ± 0.16	0.78 ± 0.09	0.58 ± 0.07	0.34 ± 0.03	0.68 ± 0.01
stomach	5.76 ± 0.89	4.33 ± 0.75	3.20 ± 0.86	1.55 ± 0.54	3.36 ± 0.37
intestines	2.68 ± 0.02	1.98 ± 0.12	1.68 ± 0.07	1.04 ± 0.22	1.74 ± 0.04
tumor/blood	2.09 ± 0.12	3.20 ± 0.44	3.24 ± 0.42	10.9 ± 3.35	0.75 ± 0.21
tumor/muscle	5.03 ± 0.03	5.20 ± 0.71	3.83 ± 0.07	5.16 ± 0.39	1.40 ± 0.49

Table 2. Radioactivity, Expressed as Percent Injected Dose per Gram Tissue in Different Organs and Tumor of MDA-MB-435 Xenograft Model after Intravenous Injection of 2 μCi of ^{125}I-E[c(RGDyK)]$_2$−PTX conjugate at 30 min, 1, 2, 4 h, and 1 h Block (with coinjection of 10 mg/kg c(RGDyK)) (n = 4)

	0.5 h	1 h	2 h	4 h	1 h block
blood	0.63 ± 0.09	0.58 ± 0.01	0.23 ± 0.06	0.07 ± 0.01	0.44 ± 0.05
muscle	0.29 ± 0.04	0.47 ± 0.01	0.58 ± 0.11	0.39 ± 0.01	0.14 ± 0.02
tumor	0.97 ± 0.24	1.91 ± 0.09	2.72 ± 0.16	2.37 ± 0.76	0.42 ± 0.07
bone	1.14 ± 0.01	1.77 ± 0.73	1.81 ± 0.73	0.83 ± 0.12	0.41 ± 0.09
heart	0.81 ± 0.12	0.82 ± 0.05	0.99 ± 0.05	0.81 ± 0.14	0.37 ± 0.01
lung	0.63 ± 0.11	1.55 ± 0.97	2.36 ± 0.97	1.38 ± 0.20	0.95 ± 0.03
liver	3.59 ± 0.48	3.35 ± 0.08	5.66 ± 0.08	4.25 ± 0.52	2.43 ± 0.38
kidney	3.33 ± 0.47	3.61 ± 0.14	6.51 ± 0.14	5.53 ± 0.73	2.32 ± 0.46
spleen	1.04 ± 0.07	1.45 ± 0.24	2.53 ± 0.24	2.14 ± 0.07	0.33 ± 0.06
pancreas	0.34 ± 0.04	0.49 ± 0.05	0.55 ± 0.05	0.48 ± 0.07	0.23 ± 0.01
stomach	1.55 ± 0.02	2.06 ± 0.03	3.08 ± 0.03	2.54 ± 0.12	1.06 ± 0.17
intestines	1.24 ± 0.26	1.60 ± 0.20	2.52 ± 0.20	2.25 ± 0.15	0.45 ± 0.24
tumor/blood	1.52 ± 0.14	3.32 ± 0.21	11.9 ± 2.54	33.4 ± 4.12	0.95 ± 0.17
tumor/muscle	3.32 ± 0.34	4.03 ± 0.21	4.76 ± 0.64	3.01 ± 0.954	3.02 ± 0.36

percentage of sub-G_0/G_1 population as determined by flow cytometry (50% for PTX−RGD versus 20% for PTX and PTXSX at 24 h; Figure 5). These data may suggest an enhancement of the apoptotic signaling due to the conjugation of RGD to PTX. It is expected that the same conjugate, when applied to integrin negative cancer cells, would not have similar potency due to the lack of integrin-targeted delivery, and internalization of PTX. Further studies are required to support this hypothesis. It is noteworthy that the metabolic stability of PTX−RGD conjugate and PTXSX is unknown. If the RGD conjugate and the paclitaxel hemisuccinate ester are susceptible for enzymatic degradation, the release of free paclitaxel may partially account for the cytotoxic effects observed.

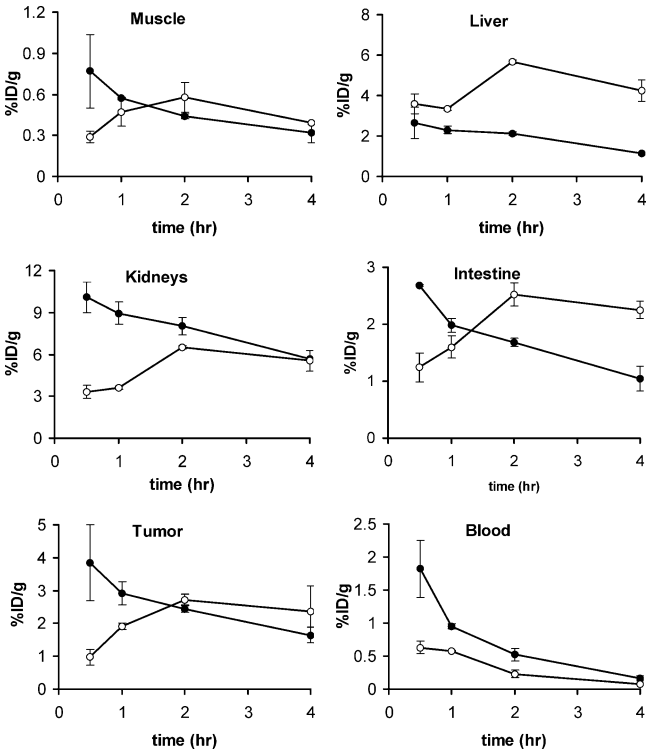

Figure 8. Comparison of biodistribution data for ^{125}I-E[c(RGDyK)]2 (●) and ^{125}I-RGD−PTXSX (○) in orthotopic MDA-MB-435 breast cancer xenograft model. Error bars denote SD (n = 4).

RGD also inhibited cell cycle proliferation by inducing G_0/G_1 arrest with the subsequent disappearance of G_2/M peak. No apoptosis was observed after cell cycle arrest. Therefore, RGD induced inhibition of cell growth was not associated with cell death, despite the alteration of cell adhesion in this cell line (cell detachment, data not shown). The conjugation of RGD to PTX, however, completely abolished the G_0/G_1 arrest induced by RGD, leading to a characteristic G_2/M-phase arrest similar to that induced by PTX. The conjugation also resulted in a decrease in alteration of cell adhesion and a subsequent increase of cell cytoxicity.

Cell cycle-specific action of PTX and RGD supports the rationale for combining both drugs and exploiting them for cancer therapy. Therefore, we evaluated the cytotoxic effects of different combination schedules (concomitant or sequential) between PTX and RGD. We also compared the efficacy of these combinations versus the conjugate. Our results showed that the efficacy of this combination is schedule-dependent. Pretreatment with RGD followed by PTX is more cytotoxic than the

other two schedules (simultaneous RGD + PTX, and reverse sequence, PTX→RGD). Therefore, from our combination studies, we can conclude that RGD possesses schedule-dependent antagonism on the antitumor activity of PTX in vitro, providing a rationale for the administration of two drugs in vivo. Taking into account that PTXSX exhibited similar properties to that of PTX (cytotoxicity, cell cycle retention, and apoptosis induction), we also evaluated the activity of the simultaneous combination of RGD and PTXSX. In contrast to the results with PTX, a synergistic effect was observed in this combination, suggesting that succinate modification improved the ability of PTX to enhance RGD cytotoxicity. Despite the ability of RGD and PTX or PTXSX in combination to inhibit cell growth, they are less effective in cell killing than the PTX−RGD conjugate. A greater percentage of sub-G_0/G_1 population was found when cells were exposed to PTX−RGD conjugate than to the combination of RGD and PTX or PTXSX. The conjugate also produced more early apoptotic cells than the drug combination.

Finally, we also demonstrated that the conjugated PTX did not significantly affect the integrin receptor affinity for RGD peptide, as demonstrated by the integrin binding affinity assays (Figure 7). These data indicate that conjugation could enhance tumor recognition of PTX through integrin receptor binding. The enhanced tumor recognition agrees well with the cytotoxicity of the conjugate observed by the MTT assays. Biodistribution studies also confirmed that PTX−RGD conjugate uptake was receptor-specific and comparable to the RGD uptake. Our results suggest that the presence of RGD peptide may improve the localization and internalization of PTX as well as exert its function as an antiangiogenic compound. Further studies, however, are required to elucidate the molecular mechanisms involved in the activity of this conjugate.

In conclusion, this study demonstrates that a paclitaxel−RGD peptide conjugate can be used as an antitumor agent. By targeting integrin $\alpha_v\beta_3$, it is possible to improve the tumor specificity and cytotoxic effect of paclitaxel, resulting in lower systemic doses to obtain anitumor efficacy and reduced toxicity. It is unknown if and when the free paclitaxel is released during the time course of the assay. The possibility of partial distribution of free drug generated through either extracellular or intracellular proteases cannot be completely ruled out. Nevertheless, an improved therapeutic index could be expected by tumor integrin specific delivery of at least a part of targeted pacliatxel, resulting in lower and therefore less toxic systemic doses that are necessary to obtain antitumor efficacy. Further evaluation of this lead compound in preclinical animal models for tumor growth inhibition and acute toxicity studies is currently in progress.

Experimental Section

Materials. All reagents, unless otherwise specified, were of analytical grade and purchased commercially. *N*-Hydroxysulfonosuccinimide (SNHS) and 1-ethyl-3-[3-(dimethylamino)-propyl]carbodiimide (EDC) were obtained from Sigma (St. Louis, MO). Cyclic RGD peptide c(RGDyK) was synthesized via solution cyclization of the fully protected linear pentapeptide H-Gly-Asp(OtBu)-D-Tyr(OtBu)-Lys(Boc)-Arg(Pbf)-OH, followed by TFA deprotection.[19] Dimeric RGD peptide E[c(RGDyK)]$_2$ was prepared by coupling Boc-Glu-OH with 2 equiv of monomeric RGD peptide c(RGDyK) followed by TFA cleavage.[24,25,37] PTX-2′-succinate (PTXSX) was prepared by reacting PTX (Hande Tech, Houston, TX) with equal molar amount of succinic anhydride in pyridine.[38] ^{125}I-Echistatin labeled by the lactoperoxidase method to a specific activity of 2000 Ci/mmol was purchased from Amersham Biosciences (Piscataway, NJ). Echistatin was purchased from Sigma (St. Louis, MO). Purified human integrin $\alpha_v\beta_3$ in Triton-100 formulation was obtained from Chemicon International (Temecula, CA).

E[c(RGDyK)]$_2$−PTX Conjugate. To a solution of PTXSX (5 mg, 5.25 μmol) in 50% CH_3CN (2 mL) and EDC (1 mg, 5.5 μmol) in water (500 μL) was added 0.1 N NaOH to adjust the pH to 5.0. SNHS (1.1 mg, 5 μmol) was then added to the stirring mixture on an ice-bath, and 0.1 N NaOH was further added to adjust the pH to 5.5. The reaction was allowed to proceed for 30 min at 4 °C. To the active ester PTXSX-OSSu prepared in situ was then added dimeric RGD peptide E[c(RGDyK)]$_2$ (13.5 mg, 10 μmol). The reaction was allowed to mix overnight at 4 °C. The purification of the crude product was carried out on a semipreparative reversed-phase HPLC system (Waters 515 chromatography system with a 486 tunable absorbance detector). Version 7.2.1 Labtech Notebook/XE software (Andover, MA) was used to record chromatograms. Purification was performed on a Vydac protein and peptide column 218TP510 (5 μm, 250 × 10 mm). The flow was 5 mL/min, with the mobile phase starting from 70% solvent A (0.1% TFA in water) and 30% solvent B (0.1% TFA in acetonitrile) (0−2 min) to 10% solvent A and 90% solvent B at 32 min. The analytical HPLC method was performed with the same gradient system, but with a Vydac 218TP54 column (5 μm, 250 × 4.6 mm) at a flow rate of 1 mL/min. The absorbance was monitored at 218 nm. The fractions containing the RGD conjugate were collected and lyophilized, and the solid was dissolved in DMSO at a concentration of 10 mg/mL for use in radiolabeling reactions and in vitro assays. MALDI-TOF MS: m/z = 2285.63 for $[M + H]^+$ ($C_{110}H_{139}N_{20}O_{34}$). The retention time on analytical HPLC under the conditions defined in the Experimental Section was 12.5 min, and the yield was 45% with a purity of 97%. The retention times for PTX and PTXSX under the same gradient condition were 16.9 and 17.3 min, respectively.

^{125}I-Radiolabeling. The dimeric RGD peptide and RGD−PTX conjugate were both labeled with ^{125}I using the standard chloramine-T method.[19] The peptide (10−20 μg) was dissolved in 100 μL of phosphate-buffered saline (PBS) (pH 7.4) in a 1.5 mL polypropylene vial. [^{125}I]NaI (1 mCi) was added to the vial, followed by 150 μg of chloramine-T (10 mg/mL in PBS, pH 7.4). After 2 min, the iodination was quenched with 500 μg of $Na_2S_2O_5$ (10 mg/mL in PBS, pH 7.4). The mixture was diluted with 200 μL of 0.1% TFA and purified by analytical HPLC with collection of 0.5 mL fractions. After the solvent was removed in vacuo, the residue was triturated with water, passed through a C_{18} Sep-Pak column, washed twice with water (2 mL each), and eluted with 2 mL 80% ethanol. The ethanol was removed in vacuo, and the residue was dissolved in PBS (pH 7.4) to obtain solutions with activity concentration of 1.85 MBq/mL. The solution was passed through a 0.22 μm Millipore filter into a sterile multidose vial for use in animal experiments. Radiochemical yields of ^{125}I-E[c(RGDyK)]$_2$ and ^{125}I-RGD−PTX ranged from 50 to 60%, and radiochemical purity was over 95%.

Cell Culture. Estrogen-negative breast cancer cell line MDA-MB-435 was obtained from Dr. Francis Markland (Department of Biochemistry and Molecular Biology, University of Southern California) and was maintained as monolayer cultures in Leibovitz's L-15 medium with 2 mM L-glutamine supplemented with 10% v/v fetal bovine serum. At confluency, the cells were washed with Dulbecco's PBS and incubated at 37 °C for 5 min with trypsin−EDTA. Subsequently, the cells were detached and resuspended in new medium. All subsequent experiments were performed using cells in exponential growth.

Cytotoxicity Assay. The sensitivity of MDA-MB-435 cells

to drug was determined by MTT (3-(4,5-dimethylthiazole-2-yl)-2,5-diphenyltetrazoliumbromide) assay.[39] Briefly, 4×10^3 cells/well were seeded in 96-well plates and allowed to attach overnight. Serial dilutions of each drug were added for 48 h. An MTT solution (at a final concentration of 0.5 mg/mL) was then added to each well, and cells were incubated for 4 h at 37 °C. After removal of the media, DMSO was added to dissolve the crystals, and the absorbance was measured at 570 nm. All assays were performed in triplicate. Doses for each fraction of survival (ranging from 10% to 90% of cell viability) were determined by median-effect line method. IC_{50} (dose of each drug that inhibits 50% of cell growth) was used for the combination analysis.

Drug Combination Studies. To define the best combination between PTX and RGD, three different schedules of administration were performed: (1) PTX + RGD (48 h), (2) PTX (48 h) → RGD (24 h), and (3) RGD (48 h) → PTX (24 h). Cell viability for each combination was assessed by MTT assay and data were analyzed by Chou and Talalay method.[40] Briefly, the analyses of combined drug effects were performed in each experiment with serial dilutions of both drugs administered at doses that typically correspond to $^1/_4$, 1/2, 1, 1.5, and 3 times the individual IC_{50} values. Fractional survival was then calculated by dividing the number of cells in drug-treated plates by the number of cells in control plates. Data were subsequently analyzed by the method of Chou and Talalay.[40] By using this method it is possible to calculate the doses of the individual drugs and the combination required to produce varying levels of cytotoxicity. For each level of cytotoxicity, a parameter called the combination index (CI) is then calculated according to the following equation: $CI_f = D_1/(D_f)_1 + D_2/(D_f)_2 + \lambda D_1D_2/(D_f)_1(D_f)_2$,[39] where D_1 and D_2 are the concentrations of the combination required to produce survival f. $(D_f)_1$ and $(D_f)_2$ are the concentrations of the individual drugs required to produce f. The value for λ was set to one or zero depending on whether the drugs are assumed to be mutually nonexclusive or mutually exclusive, respectively, in their action. According to this method, synergism is indicated by a CI < 1, antagonism by a CI > 1, and additivity by CI = 1.

Cell Cycle Analysis. Cell cycle perturbations induced by RGD, PTX, PTXSX, PTX−RGD conjugate or the combination of PTX and RGD were analyzed by propidium iodide (PI) DNA staining. Briefly, exponentially growing MDA-MB-435 cells were treated with IC_{80} doses of each drug (sequential combinations) for 24, 48, and 72 h. At the end of each treatment, cells were collected and washed with PBS after a gentle centrifugation at 200*g* for 5 min. Cells were thoroughly suspended in 0.5 mL of PBS and fixed in 70% ethanol for at least 2 h at 4 °C. Ethanol-suspended cells were then centrifuged at 200*g* for 5 min and washed twice in PBS to remove residual ethanol. For cell cycle analysis, the pellets were suspended in 1 mL of PBS containing 0.02 mg/mL of PI, 0.5 mg/mL of DNase-free RNase A and 0.1% of Triton X-100 and incubated at 37 °C for 30 min. Cell cycle profiles were studied using a FACScan flow cytometer (Becton Dickinson, San Jose, CA) and data were analyzed by ModFit LT software (Verity Software House Inc).

Apoptosis Assay. To quantify the drug-induced apoptosis, annexin V/PI staining was performed followed by flow cytometry. Briefly, after drug treatments (IC_{80} for each drug for 72 h), both floating and attached cells were collected and subjected to annexin V/PI staining using annexin V-FITC Apoptosis Detection Kit (BioVision, Palo Alto, CA) according to the protocol provided by the manufacturer. In cells undergoing apoptosis, annexin V binds to phosphatidylserine which is translocated from inner to outer leaflet of the cytoplasmatic membrane.[41] PI is used to distinguish between viable, early apoptotic, and necrotic or late apoptotic cells.[42,43] The resulting fluorescence was measured by flow cytometry using a FACScan flow cytometer (Becton Dickinson, San Jose, CA).

Receptor Binding Assay. Binding affinity of the dimeric RGD peptide−PTX to $\alpha_v\beta_3$ integrin on the surface of MDA-MB-435 cells was determined in competitive binding experiments using ^{125}I-labeled echistatin as radioligand as described in the literature with modifications.[44] In brief, MDA-MB-435 cells were harvested, washed twice with PBS, and resuspended (2×10^6 cells/mL) in binding buffer (20 mM Tris, pH 7.4, 150 mM NaCl, 2 mM $CaCl_2$, 1 mM $MgCl_2$, 1 mM $MnCl_2$, 0.1% BSA). 96-well multiscreen DV plate (filter pore size: 0.65 μm, Millipore, Billerica, MA) was incubated with ^{125}I-echistatin (50 000 cpm/well) in the presence of increasing concentrations of different RGD peptide analogues (0−1000 nM). The total incubation volume was adjusted to 200 μL. After the cells were incubated for 3 h at room temperature, the plate was filtered through multiscreen vacuum manifold and washed twice with cold binding buffer. The hydrophilic PVDF filters were collected, and the radioactivity was determined using NaI(Tl) gamma counter (Packard, Meriden, CT). The best-fit IC_{50} values for the MDA-MB-435 cells were calculated by fitting the data by nonlinear regression using GraphPad Prism (GraphPad Software, Inc., San Diego, CA). Experiments were carried out with triplicate samples.

Animal Model. All animal experiments were performed in compliance with the Guidelines for the Care and Use of Research Animals established by the University of Southern California's Animal Studies Committee. Female athymic nude mice (*nu/nu*) were obtained from Harlan (Indianapolis, IN) at 4−6 weeks of age and were kept under sterile conditions. The MDA-MB-435 cells were harvested and suspended in sterile PBS at a concentration of 5×10^7 viable cells/mL. Viable cells (5×10^6) in sterile PBS (100 μL) were injected orthotopically in the right mammary fat pad. Palpable tumors appeared by day 10−14 post-implantation. The tumors were allowed to grow 4−5 weeks until 0.5−1 g in weight. Tumor growth was followed by caliper measurements of perpendicular measures of the tumor. The weight in mg was estimated by the formula: tumor weight = $a(b^2)/2$, where a and b are the tumor length and width respectively in mm.[45]

Biodistribution. Orthotopic MDA-MB-435 tumor-bearing female athymic nude mice ($n = 4$ per time point) were injected with ^{125}I-E[c(RGDyK)]$_2$ or ^{125}I-E[c(RGDyK)]$_2$−PTX via the tail vein. The animals were euthanized at 0.5, 1, 2, and 4 h postinjection. The blocking experiment was performed by coinjecting radiotracer with a blocking dose of c(RGDyK) (10 mg/kg) and sacrificed at 1 h postinjection. Following euthanization, blood, tumor, and the major organs and tissues were collected, wet-weighed, and counted in a γ-counter (Packard). The percent injected dose per gram (% ID/g) were calculated by comparison with standards representing the injected dose per animal. Values are reported as mean ± standard deviation (SD).

Statistical Analysis. The data are expressed as means ± SD. One-way analysis of variance (ANOVA) was used for statistical evaluation. Means were compared using Student *t* test. A P value of <0.05 was considered significant.

Supporting Information Available: MALDI-TOF mass spectrum of paclitaxel−RGD conjugate. This material is available free of charge via the Internet at http://pubs.acs.org.

References

(1) Dorr, R. T.; von Hoff, D. D. *Cancer chemotherapy handbook*, 2nd ed.; Appleton and Lange: Norwalk, 1994.
(2) Dombernowsky, P.; Gehl, J.; Boesgaard, M.; Jensen, T. P.; Jensen, B. W.; Ejlertsen, B. Treatment of metastatic breast cancer with PTX and doxorubicin. *Semin. Oncol*. **1995**, *22*(Suppl 15), 13−17.
(3) Esteva, F. J.; Valero, V.; Pusztai, L.; Boehnke-Michaud, L.; Buzdar, A. U.; Hortobagyi, G. N. Chemotherapy of metastatic breast cancer: what to expect in 2001 and beyond. *Oncologist* **2001**, *6*, 133−146.
(4) Langer, M.; Kratz, F.; Rothen-Rutishauser, B.; Wunderli-Allenspach, H.; Beck-Sickinger, A. G. Novel peptide conjugates for tumor-specific chemotherapy. *J. Med. Chem*. **2001**, *44*, 1341−1348.
(5) Safavy, A.; Bonner, J. A.; Waksal, H. W.; Buchsbaum, D. J.; Gillespie, G. Y.; Khazaeli, M. B.; Arani, R.; Chen, D. T.; Carpenter, M.; Raisch, K. P. Synthesis and biological evaluation of PTX−C225 conjugate as a model for targeted drug delivery. *Bioconjugate Chem*. **2003**, *14*, 302−310.
(6) Folkman, J. Tumor angiogenesis. *Adv. Cancer Res*. **1985**, *43*, 175−203.

(7) Jain, R. K. Molecular regulation of vessel maturation. *Nat. Med*. **2003**, *9*, 685−693.
(8) Molema, G. Tumor vasculature directed drug targeting: applying new technologies and knowledge to the development of clinically relevant therapies. *Pharm. Res*. **2002**, *19*, 1251−1258.
(9) Cristofanilli, M.; Charnsangavej, C.; Hortobagyi, G. N. Angiogenesis modulation in cancer research: novel clinical approaches. *Nat. Rev. Drug Discovery* **2002**, *1*, 415−26.
(10) MacDonald, T. J.; Taga, T.; Shimada, H.; Tabrizi, P.; Zlokovic, B. V.; Cheresh, D. A.; Laug, W. E. Preferential susceptibility of brain tumors to the anti-angiogenic effects of an α_v integrin antagonist. *Neurosurgery* **2001**, *48*, 151−157.
(11) Burke, P. A.; DeNardo, S. J.; Miers, L. A.; Lamborn, K. R.; Matzku, S.; DeNardo, G. L. Cilengitide targeting of $\alpha_v\beta_3$ integrin receptor synergizes with radioimmunotherapy to increase efficacy and apoptosis in breast cancer xenografts. *Cancer Res*. **2002**, *62*, 4263−4272.
(12) Sacco, M. G.; Soldati, S.; Mira Cato E.; Cattaneo, L.; Pratesi, G.; Scanziani, E.; Vezzoni, P. Combined effects on tumor growth and metastasis by anti-estrogenic and anti-angiogenic therapies in MMTV-neu mice. *Gene Ther*. **2002**, *9*, 1338−1341.
(13) Jain, R. K. Normalizing tumor vasculature with anti-angiogenic therapy: a new paradigm for combination therapy. *Nat. Med*. **2001**, *7*, 987−989.
(14) Hynes, R. O. A reevaluation of integrins as regulators of angiogenesis. *Nat. Med*. **2002**, *8*, 918−921.
(15) Brooks, P. C.; Montgomery, A. M.; Rosenfeld, M.; Reisfeld, R. A.; Hu, T.; Klier, G.; Cheresh, D. A.Integrin $\alpha_v\beta_3$ antagonists promote tumor regression by inducing apoptosis of angiogenic blood vessels. *Cell* **1994**, *79*, 1157−1164.
(16) Brooks, P. C.; Stromblad, S.; Klemke, R.; Visscher, D.; Sarkar, F. H.; Cheresh, D. A. Anti-integrin $\alpha_v\beta_3$ blocks human breast cancer growth and angiogenesis in human skin. *J. Clin. Investig*. **1995**, *96*, 1815−1822.
(17) Buerkle, M. A.; Pahernik, S. A.; Sutter, A.; Jonczyk, A.; Messmer, K.; Dellian, M. Inhibition of the α_v integrins with a cyclic RGD peptide impairs angiogenesis, growth and metastasis of solid tumors in vivo. *Br. J. Cancer* **2002**, *86*, 788−795.
(18) Qiao, R.; Yan, W.; Lum, H.; Malik, A. B. Arg-Gly-Asp peptide increases endothelial hydraulic conductivity: comparison with thrombin response. *Am J Physiol.* **1995**, *269*, C110−C117.
(19) Chen, X.; Park, R.; Shahinian, A. H.; Bading, J. R.; Conti, P. S. Pharmacokinetics and tumor retention of ^{125}I-labeled RGD peptide are improved by PEGylation. *Nucl. Med. Biol*. **2004**, *31*, 11−19.
(20) Chen, X.; Park, R.; Tohme, M.; Shahinian, A. H.; Bading, J. R.; Conti, P. S. ^{18}F and ^{64}Cu-labeled RGD peptide for imaging breast cancer in mice with microPET. *Bioconjugate Chem*. **2004**, *15*, 41−49.
(21) Chen, X.; Park, R.; Shahinian, A. H.; Tohme, M.; Khankaldyyan, V.; Bozorgzadeh, M. H.; Bading, J. R.; Moats, R.; Laug, W. E.; Conti, P. S. ^{18}F-labeled RGD peptide: initial evaluation for imaging brain tumor angiogenesis. *Nucl. Med. Biol*. **2004**, *31*, 179−189.
(22) Chen, X.; Park, R.; Hou, Y.; Khankaldyyan, V.; Gonzales-Gomez, I.; Tohme, M.; Bading, J. R.; Laug, W. E.; Conti, P. S. MicroPET imaging of brain tumor angiogenesis with ^{18}F-labeled PEGylated RGD peptide. *Eur. J. Nucl. Med. Mol. Imaging* **2004**, *31*, 1081−1089.
(23) Chen, X.; Hou, Y.; Tohme, M.; Park, R.; Khankaldyyan, V.; Gonzales-Gomez, I.; Bading, J. R.; Laug, W. E.; Conti, P. S. PEGylated RGD peptide: ^{64}Cu-labeling and PET imaging of brain tumor angiogenesis. *J. Nucl. Med*. **2004**, *45*, 1776−1783.
(24) Chen, X.; Tohme, M.; Park, R.; Hou, Y.; Bading, J. R.; Conti, P. S. MicroPET imaging of $\alpha_v\beta_3$ integrin expression with ^{18}F-labeled dimeric RGD peptide. *Mol. Imaging* **2004**, *3*, 96−104.
(25) Chen, X.; Liu, S.; Hou, Y.; Tohme, M.; Park, R.; Bading, J. R.; Conti, P. S. MicroPET imaging of breast cancer α_v-integrin expression with ^{64}Cu-labeled dimeric RGD Peptides. *Mol. Imaging Biol*. **2004**, *6*, 350−9.
(26) Chen, X.; Conti, P. S.; Moats, R. A. In vivo near-infrared fluorescence imaging of integrin $\alpha_v\beta_3$ in brain tumor xenografts. *Cancer Res.* **2004**, *64*, 8009−8014.
(27) Haubner, R.; Wester, H. J.; Weber, W. A.; Mang, C.; Ziegler, S. I.; Goodman, S. L.; Senekowitsch-Schmidtke, R.; Kessler, H.; Schwaiger, M. Noninvasive imaging of $\alpha_v\beta_3$ integrin expression using ^{18}F-labeled RGD-containing glycopeptide and positron emission tomography. *Cancer Res*. **2001**, *61*, 1781−1785.
(28) Haubner, R.; Kuhnast, B.; Mang, C.; Weber, W. A.; Kessler, H.; Wester, H. J.; Schwaiger, M. [^{18}F]Galacto-RGD: synthesis, radiolabeling, metabolic stability, and radiation dose estimates. *Bioconjugate Chem*. **2004**, *15*, 61−69.
(29) Janssen, M. L.; Oyen, W. J.; Dijkgraaf, I.; Massuger, L. F.; Frielink, C.; Edwards, D. S.; Rajopadhye, M.; Boonstra, H.; Corstens, F. H.; Boerman, O. C. Tumor targeting with radiolabeled $_v\beta_3$ integrin binding peptides in a nude mouse model. *Cancer Res*. **2002**, *62*, 6146−6151.
(30) Xiong, J. P.; Stehle, T.; Zhang, R.; Joachimiak, A.; Frech, M.; Goodman, S. L.; Arnaout, M. A. Crystal structure of the extracellular segment of integrin $\alpha_v\beta_3$ in complex with an Arg-Gly-Asp ligand. *Science* **2002**, *296*, 151−155.
(31) Xiong, J. P.; Stehle, T.; Diefenbach, B.; Zhang, R.; Dunker, R.; Scott, D. L.; Joachimiak, A.; Goodman, S. L.; Arnaout, M. A. Crystal structure of the extracellular segment of integrin $\alpha_v\beta_3$. *Science*. **2001**, *294*, 339−345.
(32) Gottschalk, K. E.; Kessler, H. The structures of integrins and integrin-ligand complexes: implications for drug design and signal transduction. *Angew. Chem., Int. Ed*. **2002**, *41*, 3767−3774.
(33) Thumshirn, G.; Hersel, U.; Goodman, S. L.; Kessler, H. Multimeric cyclic RGD peptides as potential tools for tumor targeting: solid-phase peptide synthesis and chemoselective oxime ligation. *Chemistry* **2003**, *9*, 2717−2725.
(34) Mammen, M.; Chio, S. K.; Whitesides, G. M. Polyvalent interactions in biological systems: implications for design and use of multivalent ligands and inhibitors. *Angew. Chem., Int.* **1998**, *37*, 2755−2794.
(35) Wong, N. C.; Mueller, B. M.; Barbas, C. F.; Ruminski, P.; Quaranta, V.; Lin, E. C.; Smith, J. W. Alphav integrins mediate adhesion and migration of breast carcinoma cell lines. *Clin. Exp. Metastasis* **1998**, *16*, 50−61.
(36) Harms, J. F.; Welch, D. R.; Samant, R. S.; Shevde, L. A.; Miele, M. E.; Babu, G. R.; Goldberg, S. F.; Gilman, V. R.; Sosnowski, D. M.; Campo, D. A.; Gay, C. V.; Budgeon, L. R.; Mercer, R.; Jewell, J.; Mastro, A. M.; Donahue, H. J.; Erin, N.; Debies, M. T.; Meehan, W. J.; Jones, A. L.; Mbalaviele, G.; Nickols, A.; Christensen, N. D.; Melly, R.; Beck, L. N.; Kent, J.; Rader, R. K.; Kotyk, J. J.; Pagel, M. D.; Westlin, W. F.; Griggs, D. W. A small molecule antagonist of the $\alpha_v\beta_3$ integrin suppresses MDA-MB-435 skeletal metastasis. *Clin. Exp. Metastasis* **2004**, *21*, 119−128.
(37) Liu, S.; Cheung, E.; Ziegler, M. C.; Rajopadhye, M.; Edwards, D. S. ^{90}Y and ^{177}Lu labeling of a DOTA-conjugated vitronectin receptor antagonist useful for tumor therapy. *Bioconjugate Chem.* **2001**, *12*, 559−568.
(38) Deutsch, H. M.; Glinski, J. A.; Hernandez, M.; Haugwitz, R. D.; Narayanan, V. L.; Suffness, M.; Zalkow, L. H. Synthesis of congeners and prodrugs. 3. Water-soluble prodrugs of PTX with potent antitumor activity. *J. Med. Chem*. **1989**, *32*, 788−792.
(39) Alley, M. C.; Scudieron, D. A.; Monks, A.; Hursey, M. L.; Czerwinski, M. J.; Fink, D. L.; Abbot, B. J.; Mayo, J. G.; Shoemaker, R. H. Feasibility of drug screening with panels of human tumour cell lines using microculture tetrazolium assay. *Cancer Res.* **1988**, *48*, 589−601.
(40) Chou, T. C.; Talalay, P. Quantitative analysis of dose−effect relationships: the combined effects of multiple drugs or enzyme inhibitors. *Adv. Enzyme Regul.* **1984**, *22*, 27−55.
(41) White, E. Life, death and the pursuit of apoptosis. *Genes Dev.* **1996**, *10*, 1−15.
(42) Fadok, V. A.; Volker, D. R.; Campbell, P. A.; Cohen, J. J.; Bratton, D. L.; Henson, P. M. Exposure of the phosphatidylserine on the surface of the apoptotic lymphocytes triggers specific recognition and removal by macrophages. *J. Immunol.* **1992**, *148*, 2207−2216.
(43) Frey, T. Correlated flow cytometric analysis of terminal events in apoptosis reveals the absence of some changes in some model systems. *Cytometry* **1997**, *13*, 795−808.
(44) Kumar, C. C.; Nie, H.; Rogers, C. P.; Malkowski, M.; Maxwell, E.; Catino, J. J.; Armstrong, L. Biochemical characterization of the binding of echistatin to integrin $\alpha_v\beta_3$ receptor. *J. Pharmacol. Exp. Ther*. **1997**, *283*, 843−853.
(45) Gieseg, M. A.; Man, M. Z.; Gorski, N. A.; Madore, S. J.; Kaldjian, E. P.; Leopold, W. R. The influence of tumor size and environment on gene expression in commonly used human tumor lines. *BioMed Central Cancer* **2004**, *4*, 35.

JM049165Z